Electronic Supplementary Information for

Iron Detection and Remediation with a Functionalized Porous Polymer Applied to Environmental Water Samples

Sumin Lee,[†,+] Adam Uliana,[∬,+] Mercedes Taylor,[†] Khetpakorn Chakarawet,[†] Siva Rama Satyam Bandaru,[Γ] Sheraz Gul, [Π] Jun Xu, [∬] Cheri M. Ackerman,[†] Ruchira Chatterjee, [Π] Hiroyasu Furukawa,[†] Jeffrey A. Reimer, [∬,⊥] Junko Yano, [Π] Ashok Gadgil,[Γ] Gary J. Long,[√] Fernande Grandjean,[√] Jeffrey R. Long,*[,†,] [∬,⊥] Christopher J. Chang*[,†,‡,§,]

Departments of [†]Chemistry, [‡]Molecular and Cell Biology, [∬]Chemical and Biomolecular Engineering, [Γ]Department of Civil and Environmental Engineering, and [§]Howard Hughes Medical Institute, University of California, Berkeley, California 94720, United States

[⊥]Materials Sciences Division, and [Π]Molecular Biophysics and Integrated Bioimaging Division, Lawrence Berkeley National Laboratory, Berkeley, California 94720, United States

[√]Department of Chemistry, Missouri University of Science and Technology, University of Missouri, Rolla, Missouri 65409-0010, United States

*chrischang@berkeley.edu, *jrlong@berkeley.edu

Table of Contents

1. Synthesis of PAF-1 and PAF-1-CH_2Cl

PAF-1. Tetrakis(4-bromophenyl)methane was dried in vacuo at 80 °C overnight and used without further purification. Attempts to purify the compound before use led to PAF-1-ET samples that exhibited lower iron uptake than those prepared using as-obtained tetrakis(4-bromophenyl)methane. See Figure S1 for ^{1}H and ^{13}C NMR characterization data for the tetrakis(4-bromophenyl)methane. In a dry box, bis(1,5-cyclooctadiene)nickel(0) (2.25 g, 8.18 mmol) and dried 2,2′-bipyridyl (1.28 g, 8.18 mmol) were added to a 500 mL two-neck round-bottom Schlenk flask with anhydrous *N*,*N*-dimethylformamide (100 mL). The mixture was brought out of the dry box, and anhydrous 1,5-cyclooctadiene (1.05 mL, 8.32 mmol) was added to the solution under an Ar purge. The mixture was stirred at 80 ºC for 1 h. Tetrakis(4-bromophenyl)methane (1.00 g, 1.57 mmol) was added to the purple solution, and the mixture was stirred under Ar at 80 °C overnight to obtain a deep purple suspension. After cooling to room temperature, 6 M HCl (50 mL) was added to the mixture in air under ambient conditions. The residue was filtered and washed sequentially with warm THF (100 mL), H_2O (100 mL), ethanol (100 mL), and $CHCl_3$ (100 mL) and then dried in a vacuum oven at 170 °C to give PAF-1 as an off-white powder. Calc. for $C_{24.5}H_{16}$ (%): C 94.80, H 5.20; observed: C 92.31, H 5.45.

PAF-1-CH_2Cl. A pressure flask was charged with PAF-1 (0.20 g), paraformaldehyde (1.0 g), glacial acetic acid (6.0 mL), H_3PO_4 (3.0 mL), and concentrated HCl (20.0 mL). The flask was sealed and heated to 90 °C for 3 days. The resulting solid was filtered and washed with H_2O (500 mL), THF (100 mL), ethanol (100 mL), and $CHCl_3$ (100 mL) to give PAF-1-CH_2Cl, which was then dried in a vacuum oven at 150 °C to produce the pale yellow solid PAF-1-CH_2Cl. Calc. for $C_{26.5}H_{20}Cl_2$ (%): C 77.76, H 4.92, Cl 17.32; observed: C 75.88, H 4.63, Cl 13.6.

2. Structural Characterization of PAF-1, PAF-1-CH_2Cl, and PAF-1-ET

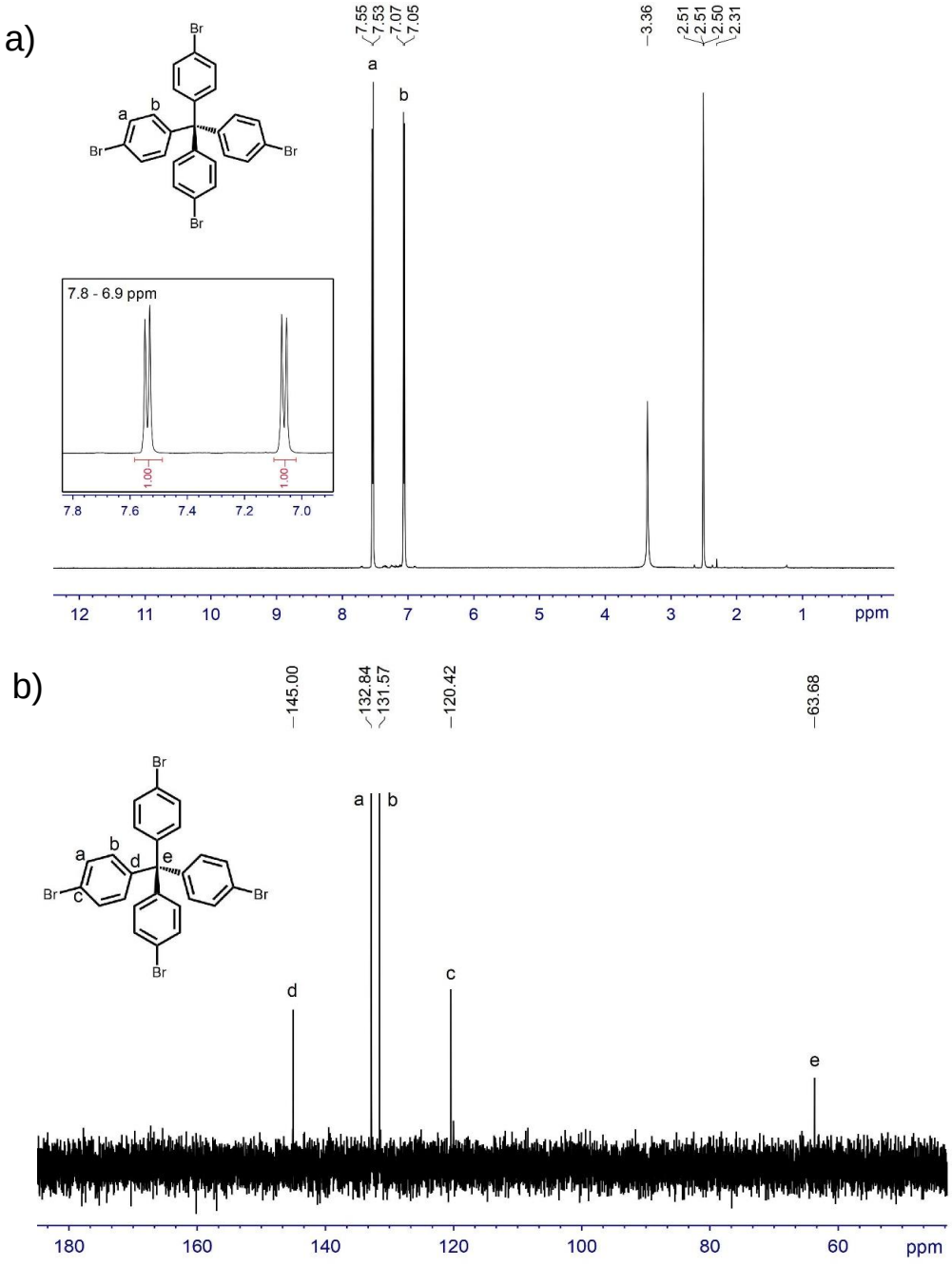

Figure S1. (a) ^{1}H and (b) ^{13}C NMR spectrum of tetrakis(4-bromophenyl)methane in DMSO-d_6. δ ^{1}H (ppm) = 7.54 (d, 2H, H-a), 7.06 (d, 2H, H-b). δ ^{13}C (ppm) = 63.68 (C-e), 120.42 (C-c), 131.57 (C-a), 132.84 (C-b), 145.00 (C-d).

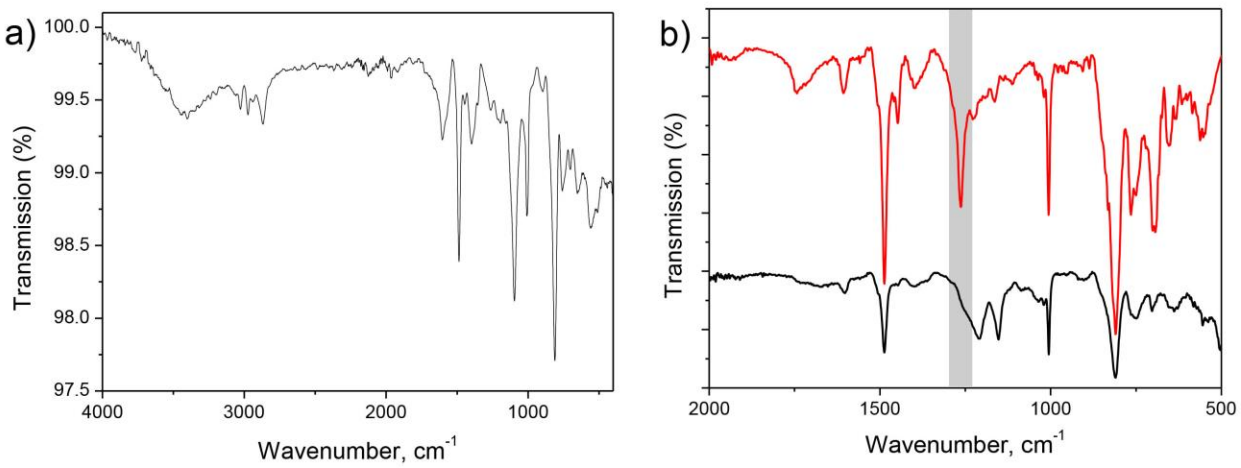

Figure S2. (a) FT-IR spectrum of PAF-1-ET and (b) a comparison of the 500-2000 cm^{-1} spectral regions for PAF-1-CH_2Cl (red) and PAF-1-ET (black). The grey band indicates the wagging mode of the –CH_2Cl group.

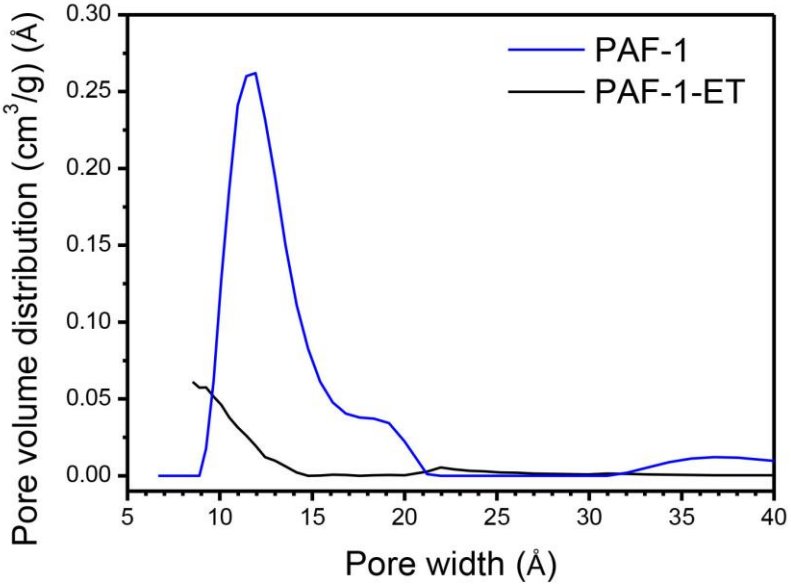

Figure S3. A comparison of the distribution of the pore volumes of PAF-1 and PAF-1-ET calculated from N_2 isotherms.

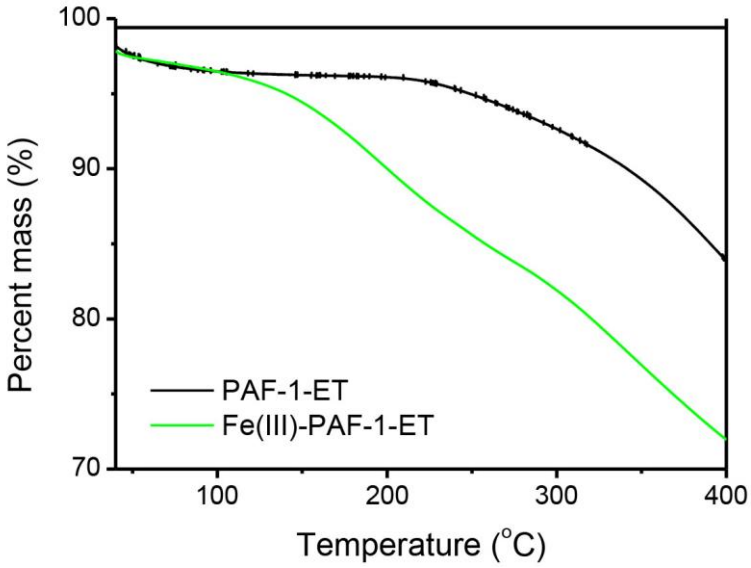

Figure S4. Thermogravimetric analysis of PAF-1-ET (black) and Fe(III)-loaded PAF-1-ET (green). The weight loss from 100 to 97% is attributed to organic solvent or water that had been adsorbed to the material and was lost below 80 °C.

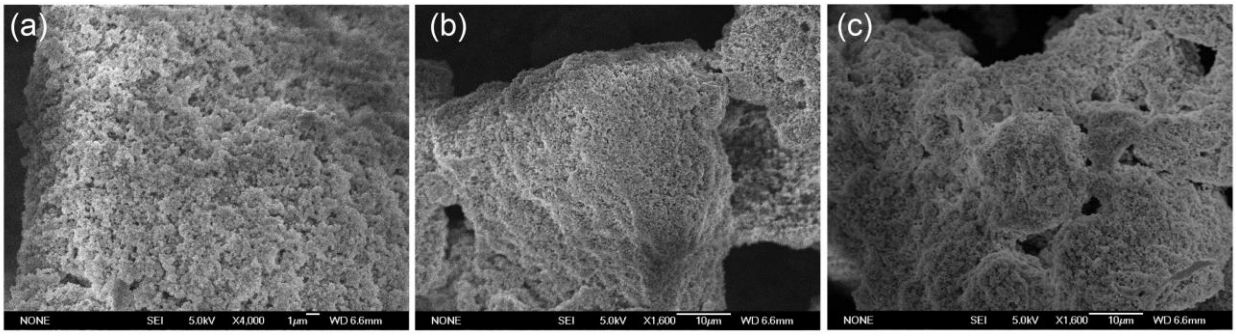

Figure S5. Scanning electron microscopy images of (a) PAF-ET (4000 magnification), (b) PAF-ET (1600 magnification), and (c) PAF-1-ET with adsorbed iron(III) (1600 magnification).

3. Determination of the Distribution Coefficient, K_d

PAF-1-ET (10.0 mg) was added to a column connected to a jar containing 1 L of a 10.3 mg/L $(NH_4)_2Fe(SO_4)_2 \cdot 6H_2O$ solution (100 mM HEPES buffer, pH 6.7). $(NH_4)_2Fe(SO_4)_2 \cdot 6H_2O$ was chosen as the initial iron source based on environmental conditions. Iron(II) is readily oxidized to iron(III) under aerobic conditions at ~pH 6.3–7.0[1,2]; therefore, within 30 min PAF-1-ET adsorbs iron(II) and iron(III) ions, but it is presumed predominantly iron(III) ions are adsorbed after 1 hour. For simplification, captured iron was thus generally referred to as being in the iron(III) state. The iron(II) and iron(III) solution was passed through PAF-1-ET with a flow rate of 0.5 mL/min. Subsequently, the initial iron solution concentration, C_i, and its filtrate concentration, C_f, were analyzed by ICP-MS to yield C_i = 10.3 mg/L and C_f = 2.7 mg/L concentrations. The quantity of iron ions adsorbed by PAF-1-ET was then calculated by subtracting the residual iron ion concentration from the initial iron ion concentration. The following equation was used to determine the distribution coefficient, K_d, for iron(III) and other adsorbed metal ions as reported in the main text:

$$K_d = \frac{(C_i - C_f)}{C_f} \times \frac{V}{m}$$

Here C_i is the initial iron ion concentration, C_f is the final equilibrium iron ion concentration, V is the volume of the treated solution in mL and m is the mass of sorbent used in g.[3,4]

The K_d values for the other metal ions (Na^+, K^+, Mg^{2+}, Ca^{2+}, Cu^{2+}, and Zn^{2+}) were determined following the same procedure above with the following conditions: PAF-1-ET (5 mg) was added into a syringe containing 45 mL of each metal solution (20 mg/L, 100 mM HEPES buffer, pH 6.7) before applying an approximate flow rate of 0.5 mL/min.

Another set of K_d values were calculated for a synthetic groundwater sample, which contained Fe^{3+}, Mg^{2+}, Ca^{2+}, and Zn^{2+} altogether in one solution. The initial concentration of each ion was 1.5, 1.1, 13, and 0.25 mg/L for Fe^{3+}, Mg^{2+}, Ca^{2+}, and Zn^{2+}, respectively. The same procedure as above was used but with the following conditions: PAF-1-ET (5 mg) was added into a syringe containing 20 mL of the synthetic groundwater solution, and a flow rate of approximately 0.5 mL/min was then applied. The final concentration of each metal ion after the PAF-1-ET addition was 0.34, 0.83, 10.8, and 0.24 mg/L for Fe^{3+}, Mg^{2+}, Ca^{2+}, and Zn^{2+}, respectively. The resulting K_d values for Fe^{3+}, Mg^{2+}, Ca^{2+}, and Zn^{2+} were calculated as 1.4×10^4, 1.3×10^3, 8.1×10^2, and 1.7×10^2 mL/g, respectively.

4. Effect of Anion on Iron Uptake

The effect of varying the counterion on iron(III) uptake by PAF-1-ET was evaluated by exposing the framework to aqueous solutions of iron(III) chloride, iron(III) sulfate hydrate, or ammonium iron(III) citrate in 100 mM HEPES buffer (two equivalent of citric acid were also added to each mixture to prevent precipitation of $Fe(OH)_3$). The iron(III) solutions were prepared with low concentrations (3.8 ppm for iron(III) chloride, 2.5 ppm for iron(III) sulfate hydrate, and 1.1 ppm for ammonium iron(III) citrate) and high concentrations (29 ppm for iron(III) chloride, 31 ppm for iron(III) sulfate hydrate, and 20 ppm for ammonium iron(III) citrate) of the metal salts. Each solution contained 2 mg of PAF-1-ET. Each mixture was stirred at room temperature overnight and then filtered through a 0.45-µm membrane filter. The filtrates were analyzed using ICP-MS to determine the remaining iron concentration. The amount of iron adsorbed by PAF-1-ET was calculated by subtracting the residual iron(III) concentration from the initial iron(III) concentration. As shown in Figure S6, PAF-1-ET showed comparable iron uptake in the presence of the different counterions, for both low and high iron concentrations.

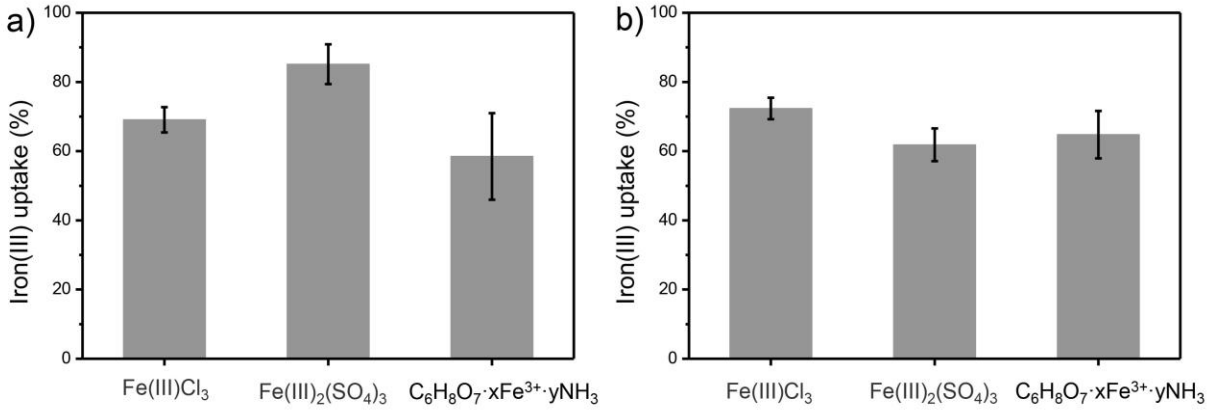

Figure S6. Comparison of the iron(III) uptake in the presence of (a) low and (b) high concentrations of chloride, sulfate, and citrate anions as discussed above.

5. Adsorption Kinetics for Iron Ion Removal by PAF-1-ET

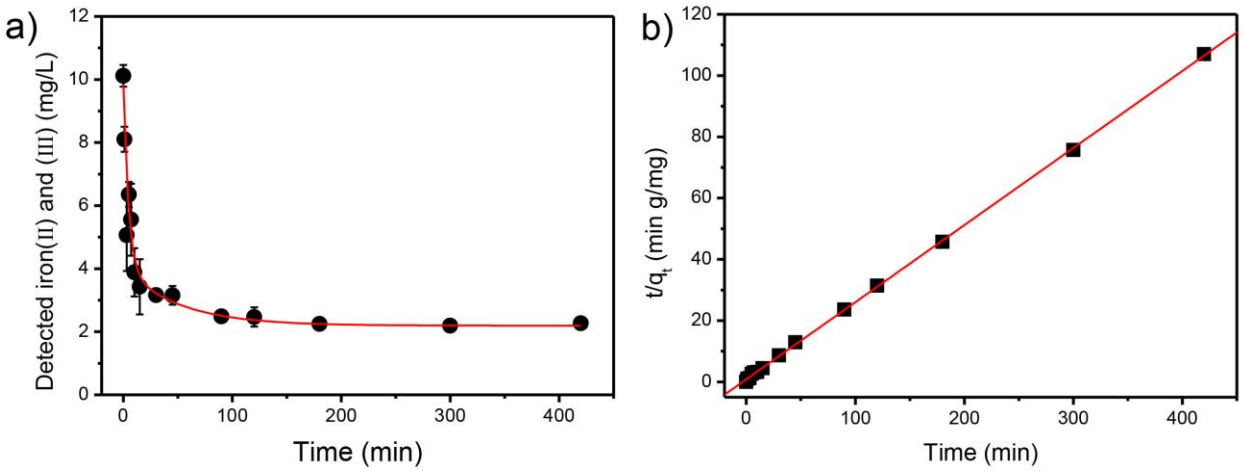

Figure S7. (a) Kinetics of the adsorption of iron(II) by PAF-1-ET from a 100 mM HEPES buffer at pH 6.7 solution of $(NH_4)_2Fe(SO_4)_2 \cdot 6H_2O$. The red line corresponds to a fit to the equation $y = Ae^{-t/t_0} + C$, where y is the detected amount of iron, A is a scale factor, C is a constant, t_0 is the decay time, and t is the elapsed time. For this fit, A = 7.0(0.5) mg/L, C = 2.2(0.04) mg/L, and t_0 = 12(2) min. (b) The linear second-order kinetics plot of the time dependence of t/q. The slope and intercept of the plot are 0.252(1) g/mg and an intercept of 0.9(2) min g/mg, respectively (correlation coefficient of –0.575 and R^2 = 0.998). The resulting pseudo-second-order rate constant, k, is 0.07(2) g/(mg min).

Table S1. Single-site Langmuir model fit parameters for iron adsorption in PAF-1-ET and PAF-1-CH_2Cl.[a]

Langmuir Parameter	PAF-1-ET	PAF-1-CH_2Cl
q_{sat}, mg/g	105(4)	37(2)
K_L, L/mg	0.020(2)	0.010(1)
$q_{sat} - K_L$ correlation coefficient	−0.900	−0.979

[a]Attempted fits of the data for PAF-1-ET using a dual-site Langmuir model according to the expression $q_e = \frac{q_{sat,1}K_{L,1}C_e}{1+K_{L,1}C_e} + \frac{q_{sat,2}K_{L,2}C_e}{1+K_{L,2}C_e}$ resulted in unacceptable fit parameters. In particular, $q_{sat,2}$, and $K_{L,2}$ were undefined, and all four of the parameters were perfectly correlated, with a correlation coefficient of 1.00. The same was true for PAF-1-CH_2Cl.

6. Mössbauer Data and Analysis

The $^{57}FeCl_3$ used for loading of PAF-1-ET was prepared from a reported procedure.[5] A round bottom flask containing ^{57}Fe oxide powder (50 mg) was fitted with a reflux condenser and filled with argon. Concentrated HCl (1 mL, freeze-pump-thawed to remove O_2) was added to the flask. The solution was stirred at reflux overnight until the evolution of H_2 gas ceased and all of the ^{57}Fe oxide had dissolved. The resulting yellow/green solution was heated under vacuum to remove excess HCl and water, resulting in near quantitative yield of $^{57}FeCl_2$ dihydrate. Storage of this solid in air led to oxidation and the formation of $^{57}FeCl_3$.

Mössbauer fits for PAF-1-ET used a Lorentzian line shape and involved two quadrupole doublets representing a distribution of the local environments associated with the adsorbed Fe^{3+} ions. Preliminary fits indicated that the two quadrupole doublets always had, within their experimental uncertainty, the same isomer shift and thus the shifts were constrained to be equal in all subsequent fits. The spectral areas of these two components were also constrained to be equal because preliminary fits indicated a somewhat random temperature variation of their relative areas. The quadrupole splitting of the two doublets was found to be essentially temperature-independent. A 9% by area high-spin Fe^{2+} component, perhaps residual from the $^{57}FeCl_3$ preparation, was also observed at all temperatures (green component in Figure 4a,b in the main text and Figure S8).

In addition to the two paramagnetic quadrupole doublets observed between 300 and 50 K, at 20, 10, and 5 K the spectra also exhibit additional components due to slow paramagnetic relaxation on the Mössbauer timescale, components which were fit with the minimum number of broadened sextets needed to fit the spectral profile. As might be expected for a distribution of local iron(III) environments, quadrupole shifts of less than ~±0.3 mm/s were associated with the iron(III) sextets.

A fit of the isomer shift temperature dependence between 5 and 300 K with the Debye model for a solid (Figure S9, top) yielded a Mössbauer temperature, Θ_M, of 358(34) K. A fit of the temperature dependence of the logarithm of the spectral absorption area between 50 and 300 K with the Debye model for a solid (Figure S9, bottom) yielded a Debye temperature, Θ_D, of 141(3) K. Data points obtained at 5, 10, and 20 K were excluded from this fit because the extensive differences in the internal reabsorption of the Mössbauer γ-ray in the doublet and sextet portions of the spectra led to larger than expected areas at these temperatures. As is usually observed,[6,7] the Mössbauer temperature is two to three times higher than the Debye temperature, because the two temperatures probe different portions of the phonon spectrum. Because the isomer shift and absorption area depend on the mean-square velocity and mean-square displacement of the ^{57}Fe nuclide, respectively, there is no model-independent relationship between these two temperatures. Generally, the isomer shift temperature dependence is more sensitive to high-energy phonons. Here, both temperatures are relatively low and indicate the relative softness of the lattice around the Fe^{3+} in PAF-1-ET. It is worth noting that the vibrations probed in the Mössbauer spectra are at lower energies than those probed in the FT-IR spectra (Figure S2b).

Table S2. Iron-57 Mössbauer spectral parameters for the iron(III) in PAF-1-ET.[a]

T, K	δ, mm/s[b]	$\Delta E_Q{}^1$, mm/s	$\Delta E_Q{}^2$, mm/s	$\Delta E_Q{}^{ave}$ mm/s	Γ^{ave} mm/s[c]	Area, %
300	0.385(2)	0.61(1)	0.97(1)	0.79(1)	0.45(2)	91
200	0.443(2)	0.614(8)	0.98(1)	0.80(1)	0.45(1)	91
100	0.492(1)	0.613(5)	0.999(3)	0.803(5)	0.45(1)	91
50	0.507(1)	0.617(5)	1.000(6)	0.809(6)	0.46(1)	91
20	0.516(1)	0.673(8)	0.99(1)	0.83(1)	0.58(2)	73.4(6)
10	0.522(1)	0.597(5)	1.025(6)	0.811(6)	0.45(1)	40.6(6)
5	0.522(1)	0.594(6)	1.019(7)	0.807(7)	0.43(1)	32.2(4)

[a]Statistical fitting uncertainties are given in parentheses. More realistic uncertainties are ca. two to three times larger. The absence of an uncertainty indicates that the parameter was constrained to the value given. [b]Referenced to α-iron at 295 K. [c]The average full width at half-maximum.

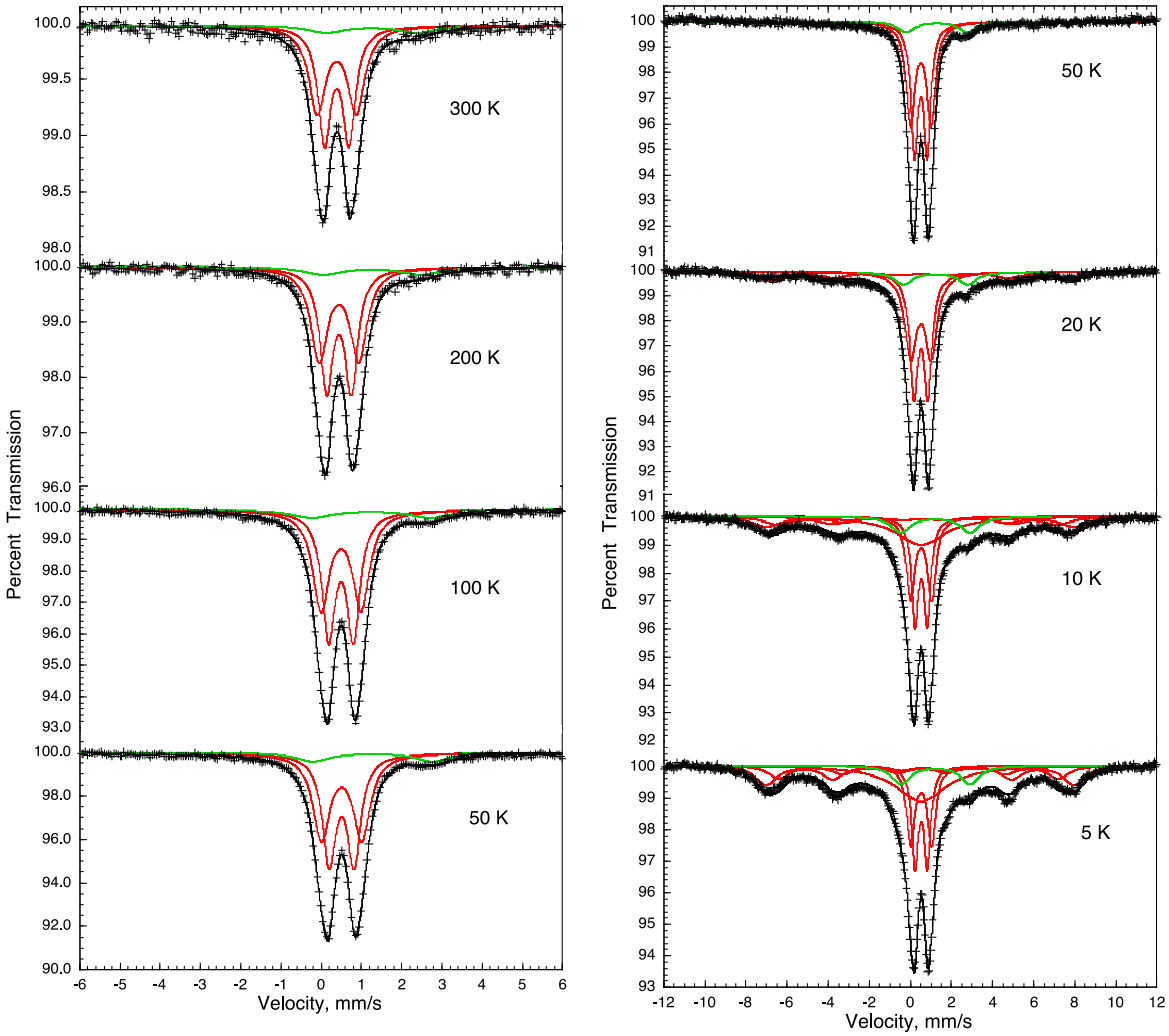

Figure S8. Mössbauer spectra of PAF-1-ET obtained at the indicated temperatures. Components assigned to iron(III) and iron(II) are shown in red and green, respectively. The total fit is shown in black.

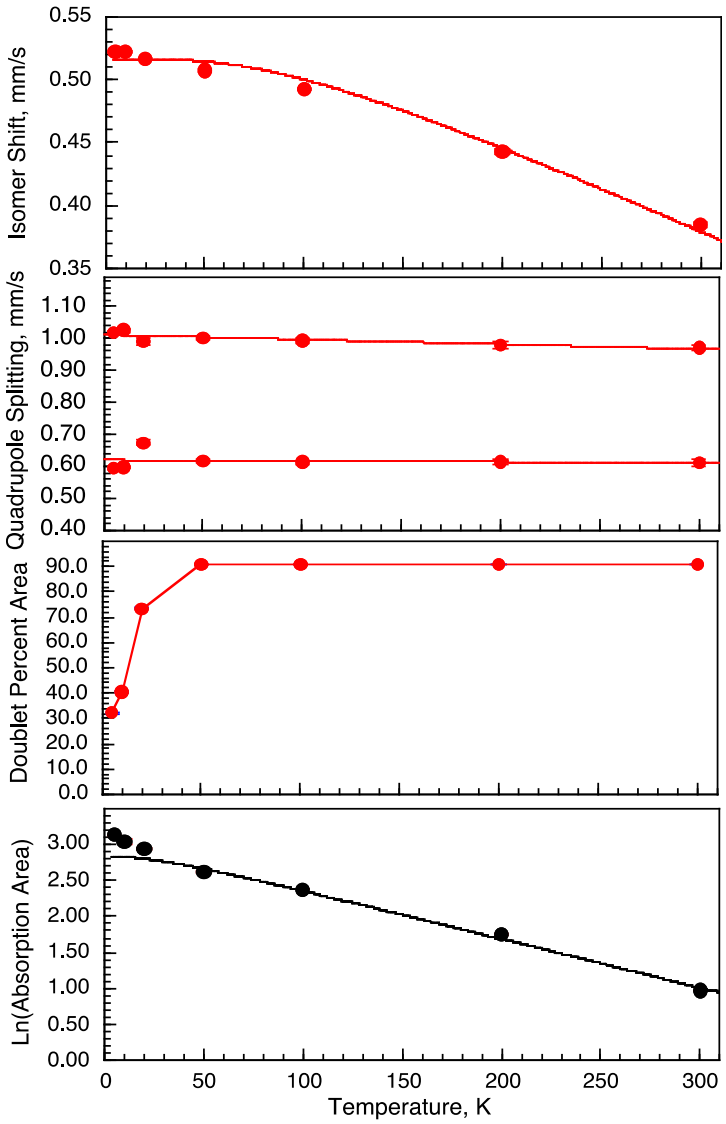

Figure S9. Top: the temperature dependence of the iron(III) isomer shift (red circles) with the Debye-model fit (red line). Second: the temperature dependence of the iron(III) quadrupole splitting, with a linear fit shown. Third: the temperature dependence of the percent area of the two iron(III) quadrupole doublets. Bottom: the temperature dependence from 300 to 50 K of the logarithm of the spectral absorption area, expressed in (%ε)(mm/s), with the Debye-model fit shown as the black line. In all four plots the uncertainties are essentially the size of the symbols.

7. X-ray Absorption and Electron Paramagnetic Resonance Spectroscopy Data

Table S3. Iron *K*-edge EXAFS fits for iron(III) adsorbed onto PAF-1-ET.[a]

Path	*R*, Å	*N*	σ^2, 10^{-3} Å^2	*R*-factor, %	ΔE_0, eV
Fe–O	2.00±0.01	6	5.98±0.59	0.65	−1.58±1.94
Fe–C	3.06±0.04	12	16.6±5.14		

[a]The fit for adsorbed iron(III) was performed for the ranges $3.46 \le k(\text{Å}^{-1}) \le 10.52$ and $1.0 \le R(\text{Å}) \le 3.1$.

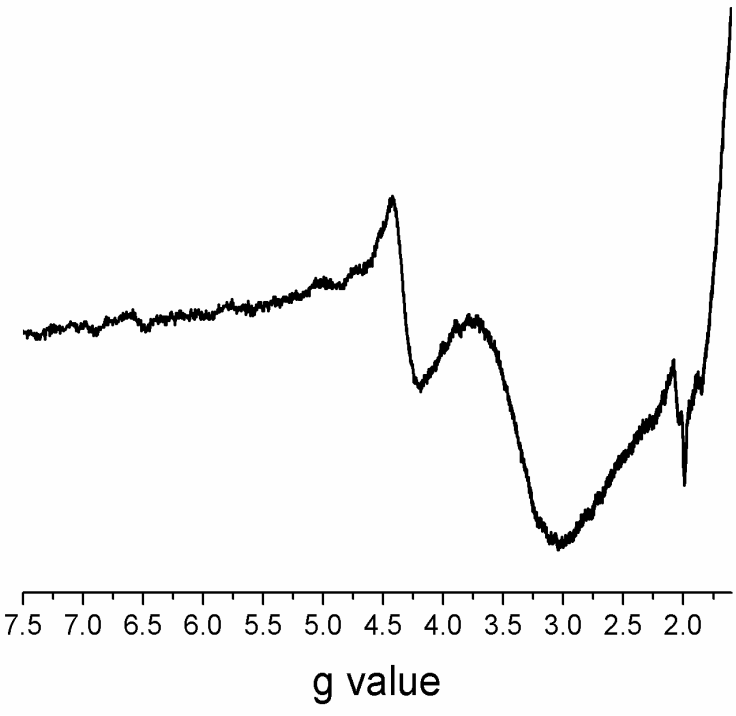

Figure S10. The derivative of the X-band of the electron paramagnetic resonance absorption spectrum of iron(III) adsorbed on PAF-1-ET measured at 8 K. The spectral absorption peak with a *g*-value of 4.3 is characteristic of $S = 5/2$ high-spin iron(III).

8. Carbon-13 Solid-state NMR Data for PAF-1-ET and Fe(III)-PAF-1-ET

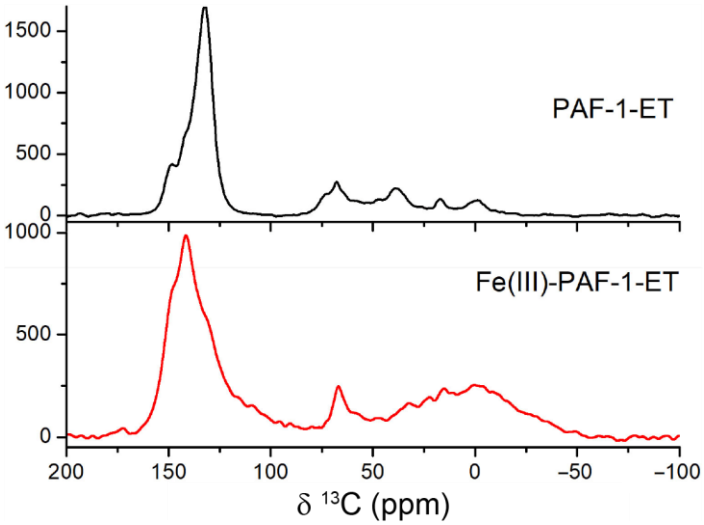

Figure S11. Comparison of the solid-state ^{13}C NMR spectra of PAF-1-ET (black) and iron(III)-PAF-1-ET (red). All ET functional group peaks present for PAF-1-ET (73, 48, 39, and 17 ppm, refer to Figure 1b in the main text for assignments) shifted upfield in iron(III)-PAF-1-ET. The peak at 67 ppm—assigned to the quaternary carbon atom connected to four phenyl rings[8]—was not affected by iron coordination.

9. Modeling Studies for Iron Coordination with Functional Groups

A hypothetical PAF-1-ET with a single diamond net was generated using the program *Materials Studio 2017 R2*. The geometry of the modeled structure was optimized with the *Forcite* module in *Materials Studio*. Structures were built assuming that no sulfur atoms coordinate to iron (based on the EXAFS data), and charge balance was afforded by coordination of one monodentate sulfate anion; oxygen atoms from water and the ET groups occupied the remaining sites

In Figure S12a-c, an ET functional group is connected to two phenyl rings attached to the same tetrahedral carbon, and the oxygen atoms of each of these two ET functional groups are able to coordinate the same iron atom. Due to the flexibility of the ET functional groups, these functionalities can be located at either 2- or 3-position of the biphenyl moieties, without disrupting their ability to coordinate the same iron atom. A third ET functional group can also coordinate the same iron atom when the three ET functionalities are located at the 2-, 2′-, and 3-positions of two biphenyl groups (Figure S12d). Furthermore, an iron ion can be coordinated by two functional groups at the 2- and 2′-positions of a single biphenyl moiety (Figure S12e). The wide range of possible ET:Fe coordination modes—as well as the likely random nature of ET functionalization throughout the PAF—would support the peak shifts and broadening observed in the ^{13}C NMR solid-state NMR spectrum for PAF-1-ET. However, because of the high porosity of pristine PAF-1, the actual framework can be partially interpenetrated. In this case, two or three ET functionalities from different nets can be coordinated to the same iron. A representative example for the iron coordination environment in the interpenetrating net is illustrated in Figure S12f. It was not possible to build a feasible structure with four ET functionalities coordinated to the same iron, due to congestion of the ET groups.

In the case of maximum iron uptake, the ET:Fe ratio is estimated to be ~1.1. To provide a possible illustration of this lower ET:Fe ratio, another model structure was prepared in which iron is coordinated by only one ET group (in addition to four water molecules and one sulfate anion). Figure S13a-b illustrate a representative portion of Fe-coordinated PAF-1-ET in different perspectives. In this structure, the ET functionality is attached to the 3-position of the tetra(biphenyl-yl)methane unit to minimize the interaction between the Fe ion and the tetrahedral carbon (given solid-state NMR data that implies the location of the iron ion is close to the benzene ring rather than the tetrahedral carbon). To stabilize the iron ions, the coordinated water molecule might weakly interact with a benzene ring (possibly via a weak CH–π interaction), which may also be related to the broadening of the signal in solid-state NMR spectra. However, we cannot fully exclude the possibility that the FeO_6 unit (i.e., $Fe(SO_4)(H_2O)_4(ET)$) is stabilized at the corner created by the tetrahedral carbon. Assuming that the structure of pristine PAF-1-ET is described as a single diamond net and half of the benzene rings are functionalized, four ET groups can be accommodated in each adamantane cage. (Figure S13c).

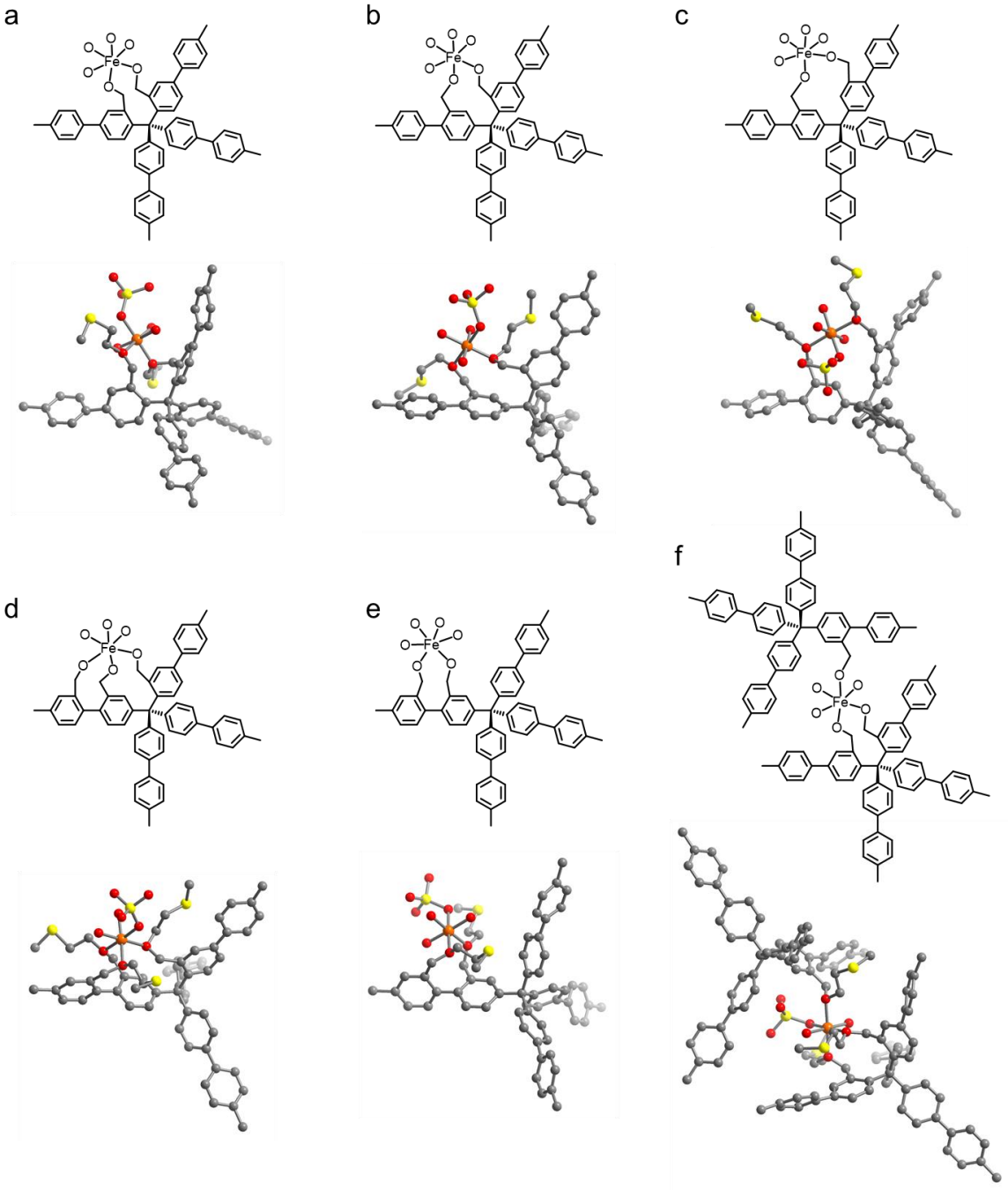

Figure S12. ChemDraw® and ball-and-stick illustrations of possible local iron coordination environments in PAF-1-ET, showing coordination of two (a-c, e) or three (d, f) ether oxygen atoms and a sulfate anion, along with two or one water molecules. Gray, red, yellow, and orange spheres represent C, O, S, and Fe atoms, respectively. Hydrogen atoms and non-coordinated ET functional groups are omitted for clarity.

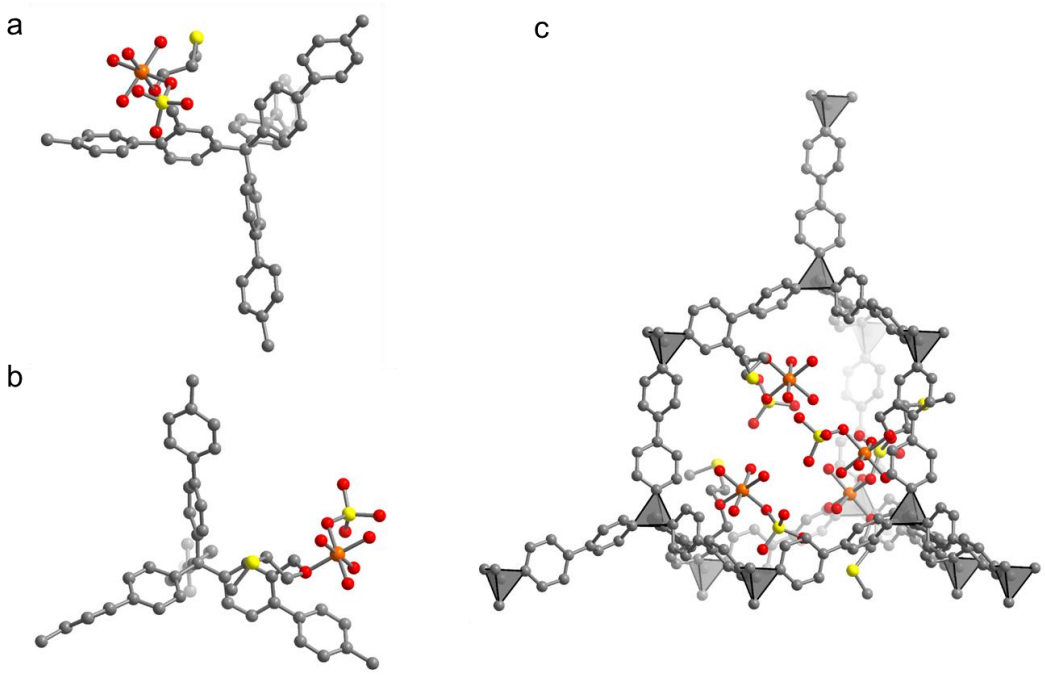

Figure S13. (a, b) Tetrahedral units extracted from the Fe-coordinated PAF-1-ET, where the ether oxygen atom coordinates with the central iron ion, along with a sulfate anion and four water molecules. The model is shown in two perspectives for clarity (a and b). (c) The adamantane cage of the same modeled structure. Four ET functionalities in the cage are shown for clarity. Atom colors are the same as those in Figure S12, while tetrahedral carbon (in the panel c) was shown in gray tetrahedra.

10. Synthesis of Derivative Polymers

PAF-1-TE. PAF-1-CH_2Cl (0.2 g) was mixed with 2-methoxyethane-1-thiol (3 equiv.) and Cs_2CO_3 (3 equiv.) in ethanol (100 mL) under N_2, and the mixture was stirred at 90 °C for 3 days.
PAF-1-OMe. Sodium methoxide (3 equiv.) was added to PAF-1-CH_2Cl (0.2 g) in methanol (100 mL) and the mixture was refluxed overnight under N_2.
PAF-1-Ethoxy. PAF-1-CH_2Cl (0.2 g) was combined with 2-methoxyethan-1-ol (3 equiv.) in tetrahydrofuran (100 mL) in the presence of NaH (3 equiv.) under N_2, and the mixture was refluxed overnight.
For each synthesis, the resulting solid was collected, washed successively with H_2O (100 mL), THF (100 mL), ethanol (100 mL), and $CHCl_3$ (100 mL), and then dried in a vacuum oven at 150 °C to produce the corresponding polymer as a grayish white powder.
Elemental analysis: **PAF-1-TE**, % calc. for $C_{32.5}H_{34}O_2S_2$: C 74.96, H 6.58, S 12.31, Cl 0.00; % observed C 74.89, H 4.81, S 5.78, Cl 0.4. **PAF-1-OMe**, % calc. for $C_{28.5}H_{26}O_2$: for C 85.26, H 6.91, Cl 0.00; % observed C 75.88, H 4.63, Cl. 0.85. **PAF-1-Ethoxy**, % calc. for $C_{32.5}H_{34}O_4$: C 79.81, H 7.31, Cl 0.00; % observed C 73.34, H 6.34, Cl 0.65.
PSF-ET. See Figure S15a below. Polysulfone (PSF, M_W = 60,000) was dried at 120 °C for 24 h before use. PSF (1.20 g) was completely dissolved in $CHCl_3$ (7.5 mL) containing zinc chloride (0.06 g). Under Ar and reflux, chloromethyl methyl ether (0.8 mL) was added dropwise. The reaction temperature was then raised to 75 °C, and the mixture was stirred for 2 h to yield a yellow liquid. The solution was added to methanol (200 mL) to precipitate the chloromethylated polymer, which was washed several times with H_2O and methanol. The resulting beige solid was dried for 24 h under vacuum (120 °C) to produce PSF-CH_2Cl (yield: 1.32 g). Subsequently, PSF-CH_2Cl (0.14 g) was mixed with 2-(methylthio)ethan-1-ol (1.0 mL) and NaH (60% in mineral oil, 0.75 g) in toluene (50 mL) under Ar and stirred at 70 °C for 3 days. The resulting solution was poured into methanol (200 mL) and then washed with H_2O (200 mL), methanol (200 mL), and hexanes (200 mL). The resulting pale yellow solid was collected and dried for 24 h under vacuum (120 °C) to produce PSF-ET (yield: 0.15 g).

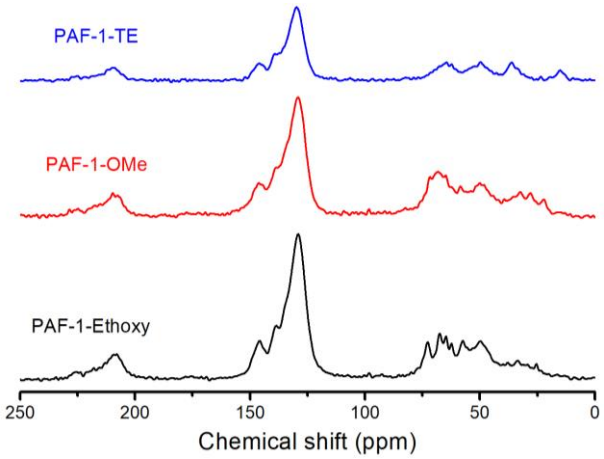

Figure S14. Solid state ^{13}C NMR spectra of PAF-1-TE, PAF-1-OMe, and PAF-1-Ethoxy.

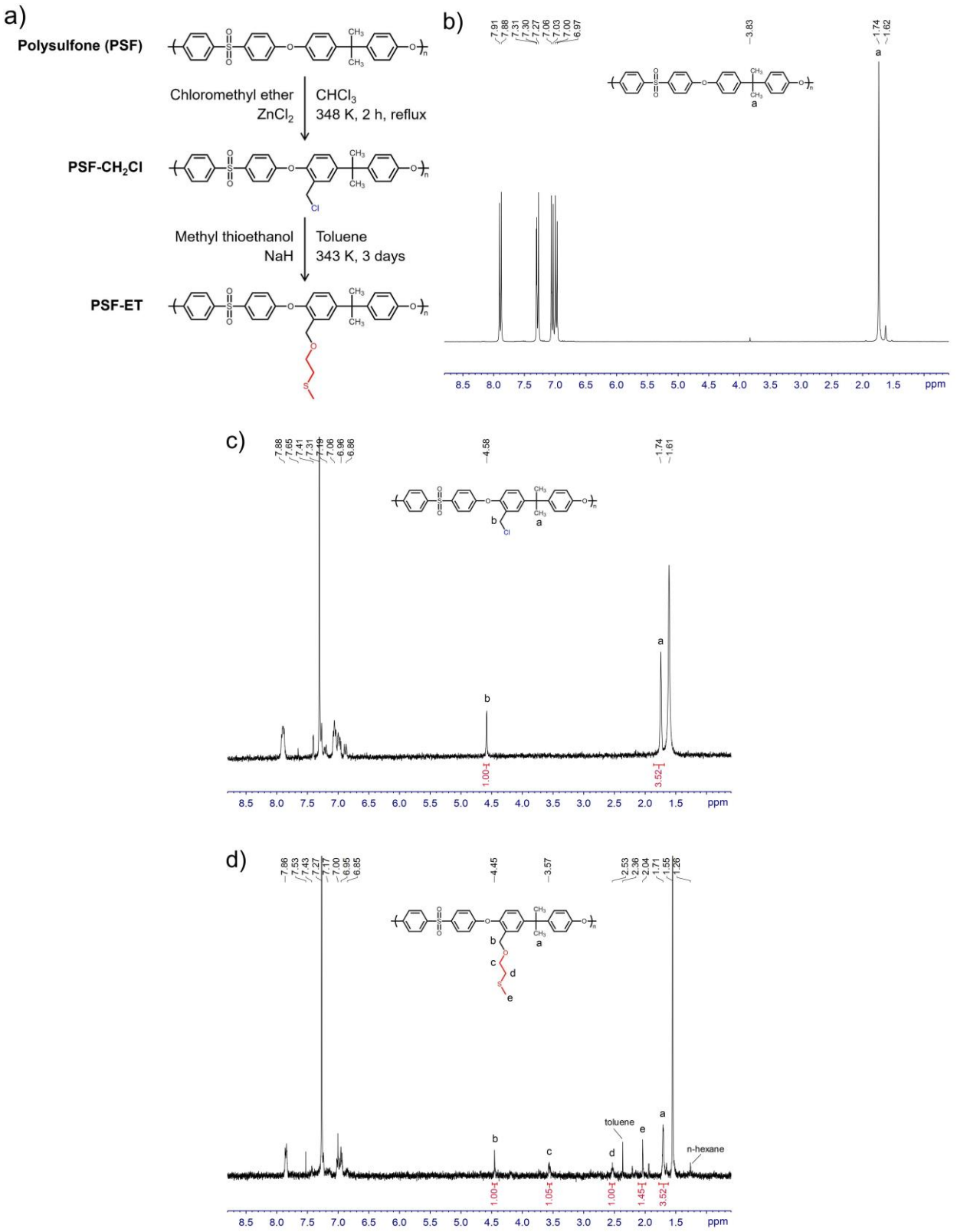

Figure S15. (a) Synthesis of PSF-ET. ^{1}H NMR spectra of (b) polysulfone (PSF) (c) chloromethylated polysulfone (PSF-CH_2Cl), and (d) ET-functionalized polysulfone (PSF-ET) in $CDCl_3$.

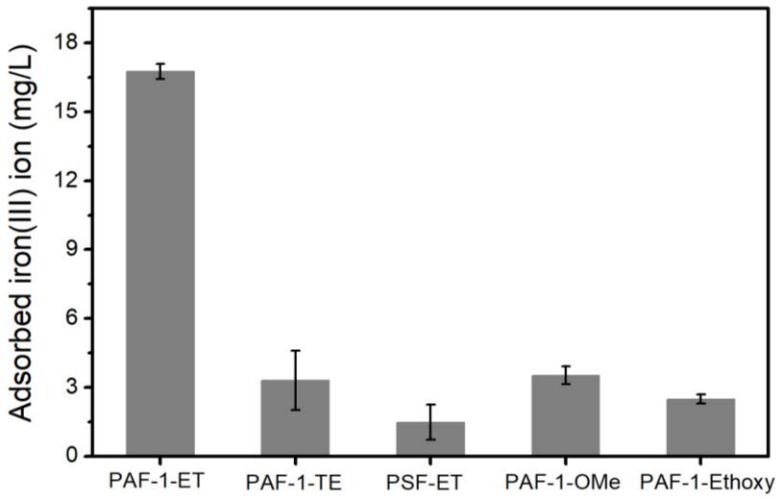

Figure S16. Iron(III) uptake comparison of PAF-1-ET, PAF-1-TE, PSF-ET, PAF-1-OMe, and PAF-1-Ethoxy in 20 mg/L $FeCl_3$ with one equivalent of citric acid to prevent precipitation of $Fe(OH)_3$ in 100 mM HEPES buffer solution at pH = 6.7.

11. Iron(III) Uptake Studies in Environmental Samples and Colorimetric Detection

Genuine groundwater collection. Environmental water samples were collected from the well head after approximately 5 min of continuous initial pumping to avoid bacterial contamination and oxygenated water. Samples were acidified immediately using HCl. As monitored with Merck ±1 pH unit test strips, the pH of the samples of raw water, and those collected after electrolysis and settling, remained near 7. This result was consistent with beaker batch tests in synthetic West Bengal, India, groundwater and field tests at the 100 L ECAR reactor in West Bengal.[9]

Other competing elements in the authentic groundwater samples have been previously reported.[9,10] Further analysis by SGS India Pvt. Ltd. (report number KE16-003637.001, report control number KER0000046121) identified the following elemental concentrations in the genuine groundwater solution: Mg 22 mg/L; Ca 144 mg/L; Cl 139 mg/L; As 0.241 mg/L; Hg 0.007 mg/L; Cd <0.003 mg/L; Cu <0.010 mg/L; Pb <0.005 mg/L; Mn 0.54 mg/L; Ni <0.01 mg/L; Se <0.005 mg/L; Mo <0.01 mg/L; B 0.04 mg/L; Zn 0.01 mg/L; Ba 0.48 mg/L; Ag <0.01 mg/L; F 0.200 mg/L; NO_3^- 0.800 mg/L; SO_4^{2-} 4.57 mg/L; CN^-, phenolic compounds, total ammonia, S^{2-}, bromoform below detection limit.

Synthetic preparation West Bengal groundwater. Concentrations of HCO_3^-, Ca^{2+}, Mg^{2+}, Si, and P of 8.2 mM, 2.6 mM, 1.9 mM, 1.3 μM, and 0.16 μM, respectively, reflected average levels in local tube wells in West Bengal according to the British Geological Survey. The target pH value of 6.6 to 7.5 was maintained throughout the experiments by adding drops of 1.1 M HCl as needed. Initial concentrations of all ions varied by less than 10% in replicate batch experiments. The samples were stored at −20 °C and freshly thawed before each experiment.

Iron(III) uptake in groundwater samples. Five synthetic iron(III) groundwater samples (5 mL each, prepared with $(NH_4)_2Fe(SO_4)_2$ in initial concentrations of 1.8, 4.7, 6.7, and 37 mg/L) and one genuine groundwater sample (14 mg/L iron(III)) were individually placed in 15 mL tubes containing 10 to 15 mg/L of citric acid and 2 mg of PAF-1-ET. Water samples with and without PAF-1-ET were kept in a shaker at room temperature overnight, filtered through 0.45-μm membrane filters, and analyzed by ICP-MS to determine the remaining iron ion content. We note that the synthetic water samples were prepared with iron(II), as the iron source in groundwater is originally from rocks, where it is present as ferrous iron. Upon exposure to air, this iron(II) is oxidized to iron(III), as is expected to be the case here with the synthetic groundwater samples. The amount of iron adsorbed by PAF-1-ET—presumed to be iron(III)—was calculated by subtracting the residual iron ion concentration from the initial iron ion concentration.

Colorimetric detection. Following exposure to the above water samples, PAF-1-ET was dried while open to the air overnight. Subsequently, 1 mM of 8-hydroxyquinoline and 1 mL of DMSO were added to each PAF-1-ET sample, and the mixture was shaken three times. The solution was filtered through a 0.45-μm membrane filter and transferred into 1 × 0.5 cm^2 quartz cuvette (1.4-mL volume, Starna). Using a Varian Cary 50 spectrophotometer, the formation of a complex between the 8-hydroxyquinoline and iron ions adsorbed by PAF-1-ET was monitored based on the absorbance of the peak at 460 nm (see Figure 5 and discussion in the main text).

Determination of the iron(III) detection limit. In a separate experiment, we prepared five synthetic iron(III) solutions with concentrations of 132, 190, 324, 506, and 1091 µg/L for use in determining the iron(III) detection limit using the PAF-1-ET and 8-hydroxyquinoline assay. The iron(III) uptake for each solution was determined following the same procedure as outlined above for the synthetic groundwater samples. The amount of iron(III) adsorbed from each water sample was then detected by using the colorimetric assay with 8-hydroxyquinoline and determining the absorbance of the peak at 460 nm (see Figure S17a). The process described above was repeated six times for each of the five synthetic solutions to obtain the errors shown in Figure S17b. In this figure it is clear that all the measured adsorbed iron(III) concentrations are smaller than the known initial iron(III) concentrations, as confirmed by a slope of 0.7(3), which is within its uncertainty less than one.

The detection limit for determining the amount of iron(III) in drinking water by using PAF-1-ET and the 8-hydroxyquinoline indicator is based on the three sigma method, $D = 3\sigma/k$, where D is the detection limit, σ is the square root of the sum of the squares of the residuals, and k is the slope of the least-squares fit of the measured concentration *vs*. the known concentration. For the results shown in Figure S17, where the red line has a unitless slope of 0.7(3) and an intercept of –63(60) µg/L,

$$\sigma^2 = \sum_{i=1}^{5} (x_i^{obs} - x_i^{calc})^2 = 1322$$

$$\sigma = \sqrt{\sigma^2} = 36.36$$

$$D = \frac{3\sigma}{slope} = 3(36.3)/0.7 = 150 \text{ µg/L}.$$

Hence, for PAF-1-ET and 8-hydroxyquinoline, the iron(III) detection limit is 150 µg/L.

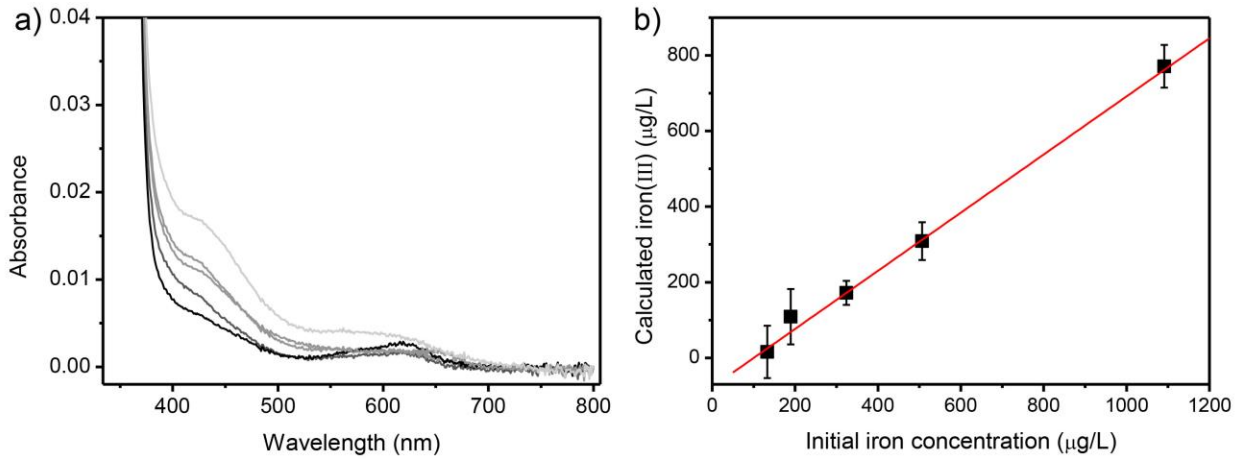

Figure S17. The detection limit for determining the amount of iron(III) in synthetic drinking water with PAF-1-ET and 8-hydroxyquinoline is based on the 3σ/*k* method. The amount of iron(III) detected with this method was independently measured (a) based on the absorbance at 460 nm of five synthetic solutions of known iron(III) concentrations (132, 190, 324, 506, and 1091 μg/L); each sample was measured six different times to obtain the adsorbed versus initial concentration plot shown in (b). The 3σ/*k* method yields a detection limit of ~150 μg/L or 0.015 mg/L.

12. Regeneration of PAF-1-ET

Iron(III)-loaded-PAF-1-ET (10 mg) was added to 100 mM of 8-hydroxyquinoline in 5 mL DMSO. The mixture was stirred at room temperature overnight to allow all bound iron(III) on PAF-1-ET to be released as a result of the formed 8-hydroxyquinoline-iron complex. The mixture was filtered through a 0.45-μm membrane filter, and the collected PAF-1-ET was washed sequentially with warm water (300 mL), THF (300 mL), ethanol (300 mL), and $CHCl_3$ (300 mL). The resulting solids were then dried in a vacuum oven at 170 ºC to yield regenerated PAF-1-ET.

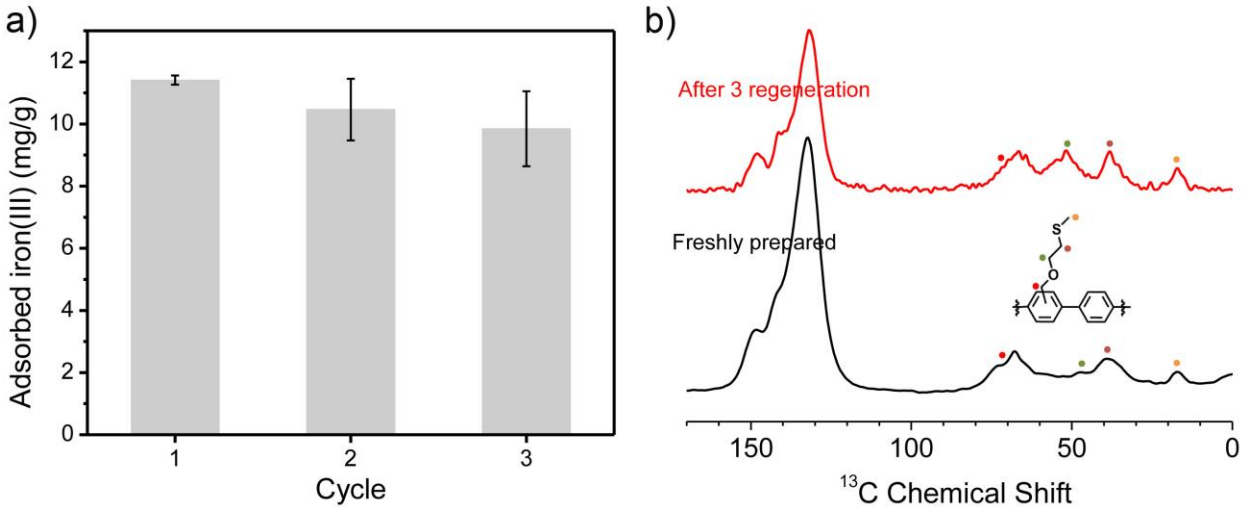

Figure S18. (a) Comparison of iron(III) ion uptake from a sample of synthetic groundwater (24 mg/mL initial concentration) by freshly prepared PAF-1-ET (cycle 1), the first regenerated polymer (cycle 2), and the second regenerated polymer (cycle 3). Regeneration was accomplished by treating the PAF with 8-hydroxyquinoline after iron adsorption. (b) Comparison of solid-state ^{13}C NMR data for freshly synthesized PAF-1-ET (black) and the second regenerated PAF-1-ET sample after cycle 3 (red).

13. References

(1) W. Stumm and G. F. Lee, *Ind. Eng. Chem.*, 1961, **53**, 143–146. https://doi.org/10.1021/ie50614a030.

(2) D. J. Kosman, *Coord. Chem. Rev.*, 2013, **257**, 210–217. https://doi.org/10.1016/j.ccr.2012.06.030.

(3) G. E. Boyd, A. W. Adamson and L. S. Myers, *J. Am. Chem. Soc.*, 1947, **69**, 2836–2848. https://doi.org/10.1021/ja01203a066.

(4) K. A. K. Ebraheem and S. T. Hamdi, *React. Funct. Polym.*, 1997, **34**, 5–10. https://doi.org/10.1016/S1381-5148(97)00077-1.

(5) T. C. Berto, M. B. Hoffman, Y. Murata, K. B. Landenberger, E. E. Alp, J. Zhao and N. Lehnert, *J. Am. Chem. Soc.*, 2011, **133**, 16714–16717. https://doi.org/10.1021/ja111693f.

(6) T. Owen, F. Grandjean, G. J. Long, K. V. Domasevitch and N. Gerasimchuk, *Inorg. Chem.*, 2008, **47**, 8704–8713. https://doi.org/10.1021/ic8004322.

(7) G. K. Shenoy, F. E. Wagner and G. M. Kalvius, Mössbauer Isomer Shifts; G. K. Shenoy and F. E. Wagner, Eds.; North-Holland: Amsterdam, the Netherlands, 1978; p. 49

(8) T. Ben, H. Ren, S. Ma, D. Cao, J. Lan, X. Jing, W. Wang, J. Xu, F. Deng, J. M. Simmons, S. Qiu and G. Zhu, *Angew. Chem. Int. Ed.*, 2009, **48**, 9457–9460. https://doi.org/10.1002/anie.200904637.

(9) S. E. Amrose, S. R. S. Bandaru, C. Delaire, C. M. van Genuchten, A. Dutta, A. DebSarkar, C. Orr, J. Roy, A. Das and A. J. Gadgil, *Sci. Total Environ.*, 2014, **488–489**, 539–546. https://doi.org/10.1016/j.scitotenv.2013.11.074.

(10) C. M. van Genuchten, S. R. S. Bandaru, E. Surorova, S. E. Amrose, A. J. Gadgil and J. Peña, *Chemosphere*, 2016, **153**, 270-279. https://doi.org/10.1016/j.chemosphere.2016.03.027.

14. Groundwater Ambient Monitoring Data from the San Francisco Bay

Summary of the groundwater collection data (see below for the full tabulated data from all 2608 wells)

Average Fe in each sample (mg/L)	Max Fe concentration (mg/L)	Std Dev of all Fe measurements (mg/L)	Number of wells with Fe content over the WHO recommended limit of 0.3 mg/L	Total number of measurements
10	950	43	1234	2608

Well ID	Average Fe (mg/L)	Std Dev (mg/L)	Number of measurements	Max Fe (mg/L)	County
L10002276721	5.1		1	5.1	Santa Clara
L10005834311	0.0	0.0	2	0.0	Alameda
L10006224883	4.8	8.5	18	31.0	Alameda
L10006514573	0.2	0.7	125	3.9	Santa Clara
L10009353957	6.0	20.1	152	117.0	Contra Costa
SL0600100443	0.0	0.0	7	0.1	Alameda
SL0600106796	16.6	29.7	10	94.0	Alameda
SL0600165101	0.0		1	0.0	Alameda
SL0604185908	0.0	0.0	2	0.0	Marin
SL0608125065	2.0	7.0	31	28.0	San Mateo
SL0608183007	15.4	10.0	4	25.0	San Mateo
SL0608587626	47.0		1	47.0	Santa Clara
SL1821Y617	0.3	0.6	40	2.7	Santa Clara
SL1823a658	115.4	240.3	15	714.0	Contra Costa
SL1823F1131	3.0	4.2	4	9.3	Santa Clara
SL1823K1135	3.7	3.8	6	8.8	Alameda
SL18244665	3.6	12.7	58	68.7	Contra Costa
SL18316736	158.1	221.0	4	470.0	Contra Costa
SL20210828	1.3	2.4	16	7.4	Contra Costa
SL20268886	0.1	0.1	2	0.2	Alameda
SL720501209	6.2	3.8	5	10.0	Santa Clara
T0600100406	24.0		1	24.0	Alameda
T0600100421	3.1	5.9	10	19.0	Alameda
T0600100939	13.8	15.2	35	65.0	Alameda
T0600100980	22.7	24.7	45	110.0	Alameda
T0600101016	4.6	5.9	32	30.0	Alameda
T0600101410	1.1	1.3	76	6.6	Alameda
T0600101476	1.3	0.9	2	2.0	Alameda
T0600101483	4.2	3.8	13	12.3	Alameda
T0600101486	0.3	0.7	16	2.6	Alameda
T0600101516	3.0	3.8	69	25.0	Alameda

T0600101803	19.4	58.4	39	370.0	Alameda
T0600101866	3.8	4.1	9	13.0	Alameda
T0600113164	1.7	1.2	7	2.8	Alameda
T0600141337	39.1	29.8	10	82.0	Alameda
T0601300335	1.3	0.5	6	1.9	Contra Costa
T0601300383	55.8	100.2	127	**950.0**	Contra Costa
T0601300404	0.0		1	0.0	Contra Costa
T060130953	20.0		1	20.0	Contra Costa
T06019741226	0.7	0.7	6	1.9	Alameda
T0608100077	40.6	60.1	25	200.0	San Mateo
T0608100147	7.5	10.9	68	57.0	San Mateo
T0608100553	0.0	0.0	4	0.0	San Mateo
T0608100572	25.6	38.8	11	130.0	San Mateo
T0608100661	3.4	4.4	42	19.0	San Mateo
T0608164698	4.4	7.0	29	27.0	San Mateo
T0608186803	13.2	15.5	2	24.2	San Mateo
T0608500255	25.6	67.4	17	270.0	Santa Clara
T0608500710	0.1	0.3	76	1.7	Santa Clara
T0608501140	2.7	3.1	8	8.4	Santa Clara
T0608501548	1.4	1.8	14	6.2	Santa Clara
T0608509697	1.3	2.8	5	6.2	Santa Clara
T0608553115	0.0	0.0	8	0.1	Santa Clara
T0608590392	25.2	35.5	7	97.0	Santa Clara
T0609592161	4.7	11.1	20	43.0	Marin
T0609592162	4.7	11.1	20	43.0	Marin
T0609700788	12.6	19.6	16	68.0	Sonoma
T0609700943	27.6	27.7	21	81.0	Sonoma
T10000000666	1.5	2.8	17	11.0	Contra Costa
T10000000901	2.5	7.5	68	56.1	Santa Clara
T10000001468	57.0	102.0	109	690.0	San Mateo
T10000002937	22.7	28.8	3	55.9	Santa Clara
T10000003206	0.9	0.8	3	1.3	Solano
T10000003434	0.6	1.0	3	1.7	Alameda
T10000003609	2.0	3.0	68	14.0	Contra Costa
T10000004547	41.3	63.8	16	240.0	Santa Clara
T10000005837	0.0	0.0	5	0.0	San Mateo
W0600103041	0.0		1	0.0	Alameda
W0600105003	0.0		1	0.0	Alameda
W0600110001	0.1	0.0	61	0.1	Alameda
W0600110003	0.1	0.4	15	1.6	Alameda
W0600110008	0.0	0.0	3	0.0	Alameda
W0600110010	0.0	0.0	41	0.0	Alameda
W0600707547	0.1		1	0.1	Contra Costa
W0600707585	0.0		1	0.0	Contra Costa
W0600707589	0.3		1	0.3	Contra Costa
W0600707594	0.0		1	0.0	Contra Costa

W0600707623	0.0		1	0.0	Contra Costa
W0600710002	0.1	0.0	3	0.1	Contra Costa
W0600710008	0.0		1	0.0	Contra Costa
W0602000573	2.4	2.6	5	6.5	Marin
W0602100518	0.0		1	0.0	Marin
W0602100519	0.2	0.1	3	0.3	Marin
W0602100549	0.0		1	0.0	Marin
W0602100565	0.1	0.0	3	0.2	Marin
W0602100579	5.2	1.3	2	6.1	Marin
W0602110006	0.0	0.1	21	0.1	Marin
W0602110007	2.0	8.7	49	60.0	Marin
W0602110008	0.7	0.7	5	1.9	Marin
W0602110302	3.7		1	3.7	No County Found
W0602110501	0.2	0.3	35	1.1	Marin
W0602110502	0.0		1	0.0	Marin
W0602702521	0.1		1	0.1	Napa
W0602800023	0.1	0.1	2	0.2	Napa
W0602800024	0.0		1	0.0	Napa
W0602800026	0.0		1	0.0	Napa
W0602800032	0.1		1	0.1	Napa
W0602800035	1.5	0.1	6	1.5	Napa
W0602800516	1.1	1.3	3	2.5	Napa
W0602800525	0.1		1	0.1	Napa
W0602800528	0.1		1	0.1	Napa
W0602800531	9.6		1	9.6	Napa
W0602800532	0.1		1	0.1	Napa
W0602800555	0.3		1	0.3	Napa
W0602800564	0.0		1	0.0	Napa
W0602800613	0.0		1	0.0	Napa
W0602800625	0.4	0.7	26	2.7	Napa
W0602800648	0.2		1	0.2	Napa
W0602800724	0.5		1	0.5	Napa
W0602801002	3.1	4.3	2	6.1	Napa
W0602801003	0.1		1	0.1	Napa
W0602801004	1.9		1	1.9	Napa
W0602801008	0.1	0.1	4	0.2	Napa
W0602801009	0.1		1	0.1	Napa
W0602801010	0.8		1	0.8	Napa
W0602801012	0.1		1	0.1	Napa
W0602801016	0.0	0.0	3	0.0	Napa
W0602801024	0.1		1	0.1	Napa
W0602801029	0.7	0.4	3	1.1	Napa
W0602801039	1.2		1	1.2	Napa
W0602801041	0.0		1	0.0	Napa
W0602801080	2.7	0.1	2	2.7	Napa
W0602810001	0.1	0.1	2	0.1	Napa

W0602810004	0.4	0.5	6	1.1	Napa
W0602810007	0.6	0.0	2	0.6	Napa
W0602810012	0.1	0.0	4	0.1	Napa
W0603301046	0.1	0.0	2	0.1	Marin
W0604100510	0.1	0.0	2	0.1	San Mateo
W0604100531	0.2	0.1	8	0.3	San Mateo
W0604100533	2.4	2.1	6	4.8	San Mateo
W0604100538	1.0	0.6	18	2.8	San Mateo
W0604100555	0.0	0.1	3	0.1	San Mateo
W0604100582	0.0		1	0.0	San Mateo
W0604110009	0.0	0.0	34	0.0	San Mateo
W0604110010	0.4	0.9	8	2.5	San Mateo
W0604110011	3.0	4.1	4	8.9	San Mateo
W0604110013	0.1	0.2	7	0.6	San Mateo
W0604110019	0.1	0.1	4	0.1	San Mateo
W0604110020	0.1	0.2	33	1.2	San Mateo
W0604110023	0.0	0.0	3	0.0	San Mateo
W0604110024	0.2		1	0.2	Santa Clara
W0604110028	3.9	1.6	27	8.5	San Mateo
W0604300522	0.0		1	0.0	Santa Clara
W0604300525	2.6	1.1	7	4.2	Santa Clara
W0604300571	0.0		1	0.0	Santa Clara
W0604300715	0.5	0.3	2	0.7	Santa Clara
W0604300716	0.7		1	0.7	Santa Clara
W0604300721	0.8		1	0.8	Santa Clara
W0604300740	3.6	5.1	2	7.2	Santa Clara
W0604300760	0.0		1	0.0	Santa Clara
W0604300770	0.1	0.1	5	0.3	Santa Clara
W0604300792	0.0		1	0.0	Santa Clara
W0604300856	0.0		1	0.0	Alameda
W0604300861	0.0		1	0.0	Santa Clara
W0604300924	0.2		1	0.2	Santa Clara
W0604300986	0.1	0.1	8	0.3	Santa Clara
W0604310001	0.0	0.2	36	1.0	Santa Clara
W0604310005	0.1		1	0.1	Santa Clara
W0604310006	0.0	0.0	3	0.0	Santa Clara
W0604310007	0.1	0.0	2	0.1	Santa Clara
W0604310011	0.2	0.3	186	2.6	Santa Clara
W0604310012	0.1	0.0	12	0.1	Santa Clara
W0604310013	0.1	0.0	3	0.1	Santa Clara
W0604310014	0.0	0.0	7	0.0	Santa Clara
W0604310018	0.0	0.0	2	0.0	Santa Clara
W0604310019	0.2	0.2	10	0.7	Santa Clara
W0604310020	0.3	0.4	13	1.3	Santa Clara
W0604410016	2.0	2.9	9	8.7	Santa Clara
W0604800511	0.5		1	0.5	Solano

W0604800574	0.0		1	0.0	Solano
W0604800596	0.3		1	0.3	Solano
W0604900533	0.2	0.1	5	0.4	Sonoma
W0604900562	0.7	1.0	11	3.0	Sonoma
W0604900563	0.1	0.1	5	0.3	Sonoma
W0604900585	0.0		1	0.0	Sonoma
W0604900843	0.3	0.4	13	1.4	Sonoma
W0604900875	0.0		1	0.0	Sonoma
W0604900901	0.3		1	0.3	Napa
W0604900909	0.0		1	0.0	Sonoma
W0604900973	0.1	0.0	2	0.1	Sonoma
W0604901061	0.0		1	0.0	Sonoma
W0604901062	0.1		1	0.1	Sonoma
W0604901080	0.4	0.2	4	0.6	Sonoma
W0604901144	0.1	0.0	2	0.1	Sonoma
W0604901275	0.0		1	0.0	Sonoma
W0604901355	0.1	0.0	2	0.1	Sonoma
W0604910006	0.2	0.2	21	0.9	Sonoma
W0604910012	0.0	0.0	7	0.1	Sonoma
W0604910013	0.1	0.2	6	0.6	Sonoma
W0604910022	0.2	0.2	2	0.4	Sonoma
W0604910025	0.1	0.0	2	0.1	Sonoma

1. Data source: http://geotracker.waterboards.ca.gov/gama/gamamap/public/default.asp?CMD=runreport&myaddress=Enter+an+address

2. Column: Average Fe show averages of the multiple measurements available for respective Well IDs in the original data source.

3. Column: Std Dev shows the standard deviation (or range for Well ID for 2 measurements) of the multiple measurements of respective wells. Blank cells have one measurement available.